



Data-driven discovery of spatiotemporal coherent patterns in pulsating soft coral tentacle motion with dynamic mode decomposition

Shuaifeng Li ¹, Liza M. Roger ², Judith Klein-Seetharaman ^{3,4}, Lenore J. Cowen ⁵,
Nastassja A. Lewinski² and Jinkyu Yang^{1,6}

¹Department of Aeronautics and Astronautics, University of Washington, Seattle, Washington 98105, USA

²Department of Chemical and Life Science Engineering, Virginia Commonwealth University, Richmond, Virginia 23284, USA

³School of Molecular Sciences, Arizona State University, Tempe, Arizona 85287, USA

⁴College of Health Solutions, Arizona State University, Phoenix, Arizona 85004, USA

⁵Department of Computer Sciences, Tufts University, Medford, Massachusetts 02155, USA

⁶Department of Mechanical Engineering, Seoul National University, Seoul, Republic of Korea



(Received 28 September 2022; accepted 8 February 2023; published 14 March 2023)

Tentacles on soft corals exhibit intriguing spatiotemporal dynamics of motions, which may benefit their survival and fitness. Despite their significance, studies of their quantitative properties still remain challenging and unexplored. Such motions are characterized by coherent patterns across both space and time, yet computational methods that address spatiotemporal dynamics are rare. Here, we introduce a data-driven method called dynamic mode decomposition (DMD) to explore the spatiotemporal behavior of tentacles of *Anthelia glauca*, where the motions of eight tentacles are captured by stereovision and object tracking techniques. The DMD reveals the stochastic motions of the tentacles, which can be well modeled as $1/f$ -type motion. Additionally, the pulsation behaviors of our soft corals are also captured by analyzing the DMD spectrum and the sliding-window DMD, where these behaviors emerge as spatial DMD modes with increased power. Finally, the impact of light conditions on the $1/f$ -type motion and pulsation behaviors is explored, where certain light conditions can manipulate the $1/f$ -type motion and emergence of pulsation behaviors. Our work, combining experimental observation and a data-driven method to characterize spatiotemporal motions of coral tentacles, paves the way to exploring the complex behaviors of individual organisms and colonies, and the effect from changing environmental variables.

DOI: [10.1103/PhysRevResearch.5.013175](https://doi.org/10.1103/PhysRevResearch.5.013175)

I. INTRODUCTION

The spatiotemporal behaviors are ubiquitous across science and engineering, including fluid dynamics, wave propagation, climate change, and animal movements. Various methods have been proposed to model and predict the spatiotemporal behaviors in numerous systems. Therein, data-driven methods, such as deep neural networks and dimensionality reduction methods, are currently being used to solve the fundamental problems including comprehending turbulent fluid dynamics and forecasting the global climate change [1–3]. One of the most powerful dimensionality reduction methods used in recent years is the dynamic mode decomposition (DMD) method because of its straightforwardness and interpretability. Given the advantages of DMD and the relation between DMD and Koopman spectral analysis, they are well suited to characterize various nonlinear physical and biological systems. DMD first obtains popularity for its ability in the fluid dynamics community to identify spatiotemporal coherent

structures from high-dimensional data [4,5]. Beyond fluid dynamics, DMD has been successfully applied to robotics [6], neurology [7,8], and epidemiology [9]. However, DMD has not yet been used to characterize the animal behaviors in biological systems.

Soft corals (Cnidaria: Octocorallia), similar to hard corals, harbor great diversity and support significant biological activities in the ocean although they are facing a severe crisis threatening their survival due to the anthropogenic activities and climate change [10]. They both host endosymbiotic dinoflagellate algae and coral colonies. However, different from the stony corals, soft corals lack calcium carbonate skeletons. Apart from differences in biological structures, there is a variety of distinctions from the perspective of spatiotemporal dynamics of motion. For example, *Montipora capricornis* (stony coral) displays imperceptible and subtle motions of tissues [11]. The polyps of *Pocillopora acuta* (stony coral) follow the fractional Brownian motion that can be affected by the environmental conditions [12].

In comparison, although rarely quantitatively studied, tentacle motions are usually studied in soft corals. Tentacles of soft corals often serve to capture food and particles in the water where the tentacles wave around and are intermittently wiped across the mouth, and as probes to locate and kill rivals [13–19]. In addition, pulsating soft corals, one type of the soft

Published by the American Physical Society under the terms of the [Creative Commons Attribution 4.0 International](https://creativecommons.org/licenses/by/4.0/) license. Further distribution of this work must maintain attribution to the author(s) and the published article's title, journal citation, and DOI.

corals, are found to have perpetual pulsation by tentacles and hence affect the surrounding fluid flow and photosynthesis of the symbionts [20–22]. The tentacles of pulsating soft corals exhibit rich dynamics of motion yet there is a lack of computational tools to characterize them. Additionally, most of the aforementioned studies about soft coral tentacle behaviors lack consideration of variable light wavelength exposure. There is also a lack of prior quantitative studies that can reveal the underlying physics. In the field of coral research in general, quantitative and physical characterization of tentacle behaviors will also help with the in-depth understanding of pulsating soft corals.

Therefore, the assistance from DMD is necessary and intriguing to explore, as it may also broaden the application of DMD and advance our understanding to pulsating soft coral behaviors in response to environmental variables. Moreover, distinct from the commonly studied pulsating *Xenia* coral, some pulsating soft corals may have subtle pulsation due to environmental conditions and inherent biological structures, which poses the challenge to identify and visualize the pulsation mode. Since DMD can provide not only dimensionality reduction in terms of a reduced set of modes, but also a model for how these modes change over time, it can help with mode identification and visualization.

Here, we investigate the tentacle motions of a pulsating soft coral, *Anthelia glauca*. The three-dimensional motions of the eight tentacles, which display a stochastic nature, are extracted by stereovision techniques [23]. We then use DMD to discover and analyze the dynamic modes with oscillations at frequencies with growth/decay rate involved in tentacle motions. The DMD spectrum and sliding-window DMD are introduced, where we discover the $1/f$ -type motion of pulsating soft coral tentacles and the spatial DMD modes with increased power in a specific frequency range. Furthermore, we visualize the exemplar DMD mode with increased power, which is confirmed to represent the pulsation behavior of our pulsating soft corals. For each tentacle, the elliptical motion with certain polarization is displayed, where correlation analysis among tentacles further indicates the collective pulsation motion of our soft coral. In addition, we investigate the emergence and frequency variation of pulsation under the effects of different light conditions. Our research, combining experimental observation techniques and a data-driven method, offers physical insights into the motions of pulsating soft coral tentacles, which will boost our understanding of pulsating soft coral behaviors and physiology. Also, this work will contribute to expanding the use of DMD to individual organisms and, potentially, their combined motion within colonies such as those formed by pulsating soft corals and their reef-building cousins.

II. EXPERIMENTAL SYSTEM

To study the motion of tentacles, we chose *Anthelia glauca* in the family of Xeniidae, a pulsating soft coral with eight long tentacles on the tubular polyps, to ensure the noticeable motion of tentacles, although *Anthelia glauca* does not pulse as much as pulsating *Xenia* coral does in the wild and in captivity.

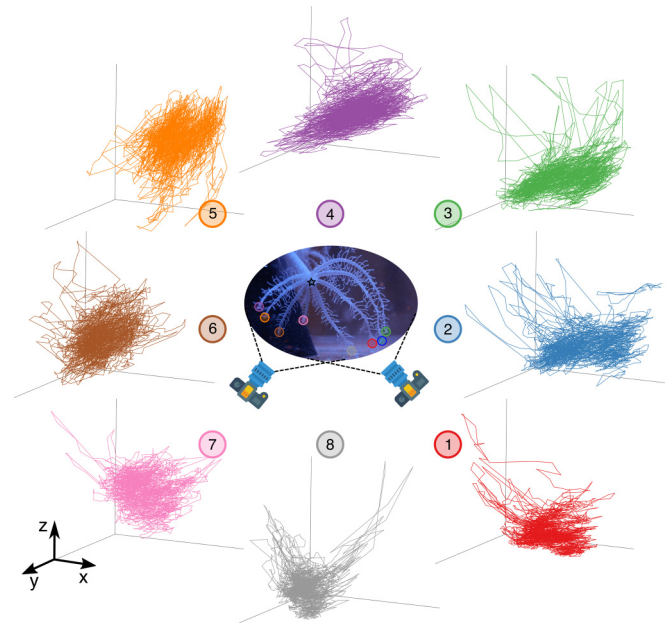


FIG. 1. The trajectories of the coral tentacles' tips in three-dimensional space. Schematic representation of the experimental setup. Stereo cameras system taking images of one polyp (eight tentacles) over 11 h is shown in the center. The trajectories of the eight tentacle tips (colored circles) are shown corresponding to the sequence number. The black star shows the position of the center of the tentacle crown (polyp mouth).

A. Experimental setup

A specimen of *Anthelia glauca* was purchased from a local store (Seattle Corals Aquariums) and was reared in a 5.68-l aquarium with specific gravity artificial seawater = 1.025 g/cm^3 and $\text{pH} = 8.4$. Regular tests on pH , NH_4^+ , NO_2^- , and NO_3^- were done to make sure the water quality was suitable for coral. The continuous water flow within the tank was provided by a Hydor Koralia Nano Aquarium Circulation Pump with a 908.5-l/h flow rate. Note that 2 h before initiating the experiment, the aquarium pump was paused to minimize the effect of water flow on spontaneous tentacle motion. The temperature of the water was controlled by the 50-W FREESEA submersible heater and was maintained in 25°C . Light was provided on a 12/12 h daylight cycle using an AI Prime 16HD Reef light system. The light used to rear our coral was mixed with 20% UV, 10% violet, 10% royal blue, 10% blue, 10% moonlight, and 10% cool white in the setting options on the AI Prime 16HD Reef light system. In the experimental study of the effect of light conditions, all aquarium settings were kept the same, except the light. The settings for blue (450–495 nm), green (495–570 nm), and red (620–750 nm) light conditions in the experiments were monochromatic with the same power as the laboratory light.

B. Stereovision system

As shown in the schematic in Fig. 1, stereovision with two synchronized cameras was used to take images of one of the polyps of *Anthelia glauca* to obtain motion information in a

three-dimensional space so that the position of each tentacle and the polyp mouth can be identified. Two synchronized cameras with lenses (Canon EOS 5D Mark IV and EF 100 mm f/2.8L Macro IS USM) were used, along with a timer to take images every 10 s. The camera settings were F10, ISO8000, and 1/200 s. The two cameras were fixed on an optical table for stability and long-period shooting for 11 h. The macro lenses of two cameras were perpendicular to the aquarium to avoid a blurred effect caused by refraction. The full time-lapse video created from the images by the two cameras is shown in Supplemental Material Movie 1 ($\times 300$ speed) [24].

Calibration and acquisition of the coefficient of direct linear transformation (DLT) were implemented by using a checkerboard pattern [23]. With the DLT method, each calibrated camera has a set of 11 coefficients that map from world coordinates to image pixel position for a single camera from a particular view, which is mathematically expressed as follows:

$$u = \frac{L_1 X_w + L_2 Y_w + L_3 Z_w + L_4}{L_9 X_w + L_{10} Y_w + L_{11} Z_w + 1}, \quad (1)$$

$$v = \frac{L_5 X_w + L_6 Y_w + L_7 Z_w + L_8}{L_9 X_w + L_{10} Y_w + L_{11} Z_w + 1}, \quad (2)$$

where (u, v) , (X_w, Y_w, Z_w) , and L_1 - L_{11} are the pixel coordinates, three dimensional (3D) coordinates, and the DLT coefficients, respectively. As long as the DLT coefficients from two camera views are obtained, the pixel coordinates of a single point in both camera views can be combined to find the corresponding 3D coordinate, which can be determined by finding the intersection of the two lines from each camera view in 3D space.

The images of the checkerboard pattern from different positions and angles are taken from both camera views. The perspective matrix \mathbf{P} that can map the world coordinates to image pixel position, which is $\mathbf{K}[\mathbf{R}|\mathbf{T}]$, can be calculated, where \mathbf{K} is the intrinsic matrix containing focal lengths and the camera's principle points. \mathbf{R} and \mathbf{T} are the rotation and translation between the world coordinate system and camera, respectively. The relation is mathematically expressed as follows:

$$s \begin{bmatrix} u \\ v \\ 1 \end{bmatrix} = \mathbf{K}[\mathbf{R}|\mathbf{T}] \begin{bmatrix} X_w \\ Y_w \\ Z_w \\ 1 \end{bmatrix}. \quad (3)$$

Finally, the DLT coefficients can be calculated after the direct relation between \mathbf{P} and the DLT coefficients from L_1 to L_{11} is found.

C. Three-dimensional coral tentacle motion

To simplify the problem, in this study, we focus on one polyp and only track the tips of eight tentacles instead of depicting the motions of the entire colony. To avoid the impact from polyp motion, we consider the relative tentacle motion with regard to the polyp mouth. Each tentacle was simplified for analysis as a line segment connecting the polyp mouth to each tip of the tentacle so that the relative position could be easily calculated. The polyp mouth and the tip of the tentacle were tracked using the correlation-based algorithm. Note that,

occasionally, the tentacles contracted into the polyp, which may be related to the feeding behaviors [13–15]. Hence, the corresponding data was missing due to the unavailable positions of tentacle tips. After the tentacle coordinates in each frame obtained by each camera were identified, the coordinates in three-dimensional space were calculated using DLT.

The trajectories of eight tentacles are illustrated in Fig. 1. All eight trajectories in three-dimensional space are stochastic and form random areas. The tentacles occasionally wander from the center of the trajectories but usually return rapidly. Some tentacles have strong motion preference along a specific direction. For example, tentacles #2, #3, and #4 exhibit a waving motion along the horizontal direction rather than vertical. Nevertheless, the featured pulsation behavior cannot be directly observed from these trajectories.

III. DMD SPECTRUM AND $1/f$ -TYPE MOTION

Since the motion of tentacles is a typical spatiotemporal behavior of pulsating soft corals, identifying these spatiotemporal patterns enables the reduction of complex measurements through projection onto coherent structures, where it may be tractable to build dynamical models and apply machine learning tools for pattern analysis. We introduce DMD as a novel and effective approach to exploring spatiotemporal patterns in pulsating soft coral tentacle motions, which combines two major advantages of current data analysis tools: power spectral analysis in time and principal components analysis in space.

After collecting the measurements (positions of tentacle tips), we constructed two $n \times (m-1)$ matrices, where n is the number of tentacles multiplied by the degrees of freedom ($n = 24$ in our study) and m is the number of snapshots over time (11 h with 10-s time intervals):

$$X = \begin{bmatrix} | & | & \cdots & | \\ x_1 & x_2 & \cdots & x_{m-1} \\ | & | & \cdots & | \end{bmatrix}, \quad X' = \begin{bmatrix} | & | & \cdots & | \\ x_2 & x_3 & \cdots & x_m \\ | & | & \cdots & | \end{bmatrix}. \quad (4)$$

These two matrices can be related by a best-fit linear operator A that minimizes the Frobenius norm error $\|X' - AX\|_F$ given by

$$X' = AX \Rightarrow A = X'X^\dagger, \quad (5)$$

where X^\dagger is the pseudoinverse of data matrix X . Usually $n \gg m$ for many systems, so, instead of obtaining A directly, we seek the eigendecomposition of A . After the decomposition of X using singular value decomposition and the rank- r truncation selection, the matrix representation \tilde{A} formed by projecting A onto the r dominant modes can be written as

$$\tilde{A} = \tilde{U}^* X' \tilde{V} \tilde{\Sigma}^{-1}, \quad (6)$$

where \tilde{U} , $\tilde{\Sigma}$, and \tilde{V} are the left unitary matrix, diagonal matrix with singular values, and right unitary matrix, respectively. The eigendecomposition of \tilde{A} results in the DMD eigenvalue λ and eigenvector W , which further derives the corresponding DMD mode ϕ being the column of $\Phi = X' \tilde{V} \tilde{\Sigma}^{-1} W$.

On the contrary, here, $n \ll m$ in data matrix X , with $n = 24$, resulting in a small number of eigenvalues that cannot fully capture the dynamics of the system [7,25]. Therefore, the augmented data matrix X_{aug} by the time-delay embedding with

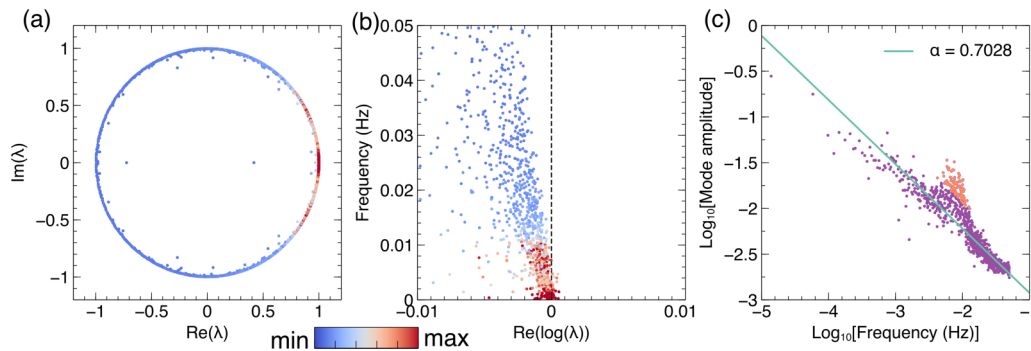


FIG. 2. DMD eigenvalues analysis and spectrum. (a) Eigenvalues λ are visualized as complex values on the complex plane with a unit circle. (b) The relation between the real part of $\log \lambda$ and frequency is displayed. The vertical black dashed line indicates that the real part of $\log \lambda$ is zero. The color in (a) and (b), which is logarithm scaled, represents the corresponding mode amplitude. (c) The mode amplitude varies as a function of frequency. The purple dots and orange dots show the modes with magnitudes within the $1/f^\alpha$ fit and larger than $0.8 \times$ standard deviations of the $1/f^\alpha$ fit. The green solid line is the fitted result using the robust regression in the form of $1/f^\alpha$.

h stacks is shown as follows:

$$X_{aug} = \begin{bmatrix} | & | & \cdots & | \\ x_1 & x_2 & \cdots & x_{m-h} \\ | & | & \cdots & | \\ x_2 & x_3 & \cdots & x_{m-h+1} \\ | & | & \cdots & | \\ \vdots & \vdots & \cdots & \vdots \\ | & | & \cdots & | \\ x_h & x_{h+1} & \cdots & x_{m-1} \\ | & | & \cdots & | \end{bmatrix}. \quad (7)$$

The X'_{aug} can be induced similarly. The DMD with the time-delay embedding aims to provide extra observables to realize the Koopman operator to accurately capture and predict the dynamics, but there is no guarantee that the resultant models are closed under the Koopman operator. Note the DMD modes are stacks of h repeats because of the shift-stacking data matrix.

Here, we choose 300 stacks to obtain the augmented data matrix to minimize the DMD reconstruction error expressed as $\frac{|X - \hat{X}|_F}{|X|_F}$, where \hat{X} is the reconstructed data matrix that will be detailed in Sec. IV, and $|\cdot|_F$ is the Frobenius norm (see Fig. S1 in the Supplemental Material [24]). Note that the DMD reconstruction error resulting from X and \hat{X} , is different from the 3D reconstruction error in stereovision that refers to the difference between the estimated and true 3D coordinates. Sufficient eigenvalues are thus obtained to capture the dynamics of the system. Each DMD mode ϕ corresponds to eigenvalue λ . The temporal dynamics, referring to growth/decay and the frequency of oscillation of each DMD mode ϕ , are reflected by the magnitude and phase of eigenvalue λ , respectively. In this case, because the raw data is strictly real, the decomposition yields complex conjugate pairs of eigenvalues and modes.

As shown in Fig. 2(a), the eigenvalues are visualized on a unit circle in the complex plane, where most are near the unit circle, suggesting most modes are oscillating with certain frequencies. A few eigenvalues are inside the unit circle, indicating the decay modes. The relation between the real parts of the logarithm eigenvalues and frequencies defined as

$f = \left| \frac{\text{imag}(\omega)}{2\pi} \right|$ where $\omega = \frac{\log \lambda}{\Delta t}$ is described in Fig. 2(b). Most real parts of the logarithm eigenvalues are slightly smaller than zero, coinciding with the observation that eigenvalues are on the unit circle in Fig. 2(a), which indicates modes with low decaying rates. The mode amplitude defined as $P = |\phi|_2^2$ is encoded by color in both Figs. 2(a) and 2(b). They both show that the modes near the zero frequency have the largest mode amplitude that declines as the frequency increases. Interestingly, another area with comparatively large amplitude near 0.008 Hz is also present, which will be discussed in the following paragraph.

Figure 2(c) gives the DMD spectrum in the logarithm-scaled graph, which displays similarities to the power spectrum. However, the power spectrum is calculated for motion of a certain tentacle along each direction independently whereas the DMD spectrum provides specific spatial modes across all tentacles. The DMD spectrum is composed of a nearly linear area and a peak area in the logarithm-scaled graph. The linear relation in the logarithm-scaled graph suggests a power-law relation between mode amplitude (P) and frequency (f) with $P \sim \frac{1}{f^\alpha}$. In this case, by using a robust linear regression to identify the outliers and peak area with comparatively large amplitude, and using reduced major axis regression to fit the DMD spectrum to obtain the reliable α , the $1/f$ -type motion is revealed where $\alpha = 0.7028$ [26]. In general, we refer colloquially to $1/f$ noise, whenever the process is modeled by $1/f^\alpha$ noise, where $0 < \alpha \leq 3$. $1/f$ noise has been prevalent in biological systems such as brain science [7,27,28] and diffusion processes [29,30]. In addition, the notable Brownian motion as well as their derived fractional Brownian motion are $1/f$ noise with $1 < \alpha < 3$.

Apart from the power-law relation marked in purple dots, the modes with increased power are illustrated as orange dots in Fig. 2(c). Note that the criteria for the detection of the modes with comparatively large amplitudes is when their power amplitudes exceed $0.8 \times$ standard deviations of the $1/f^\alpha$ fit. The frequency of this peak area is around 0.008 Hz, near which the pulsating soft coral tentacles have relatively strong oscillating motion.

Similar to the idea of a spectrogram in Fourier analysis, we introduce sliding-window DMD to analyze the DMD spectrum variation over time. Here, the width of the sliding

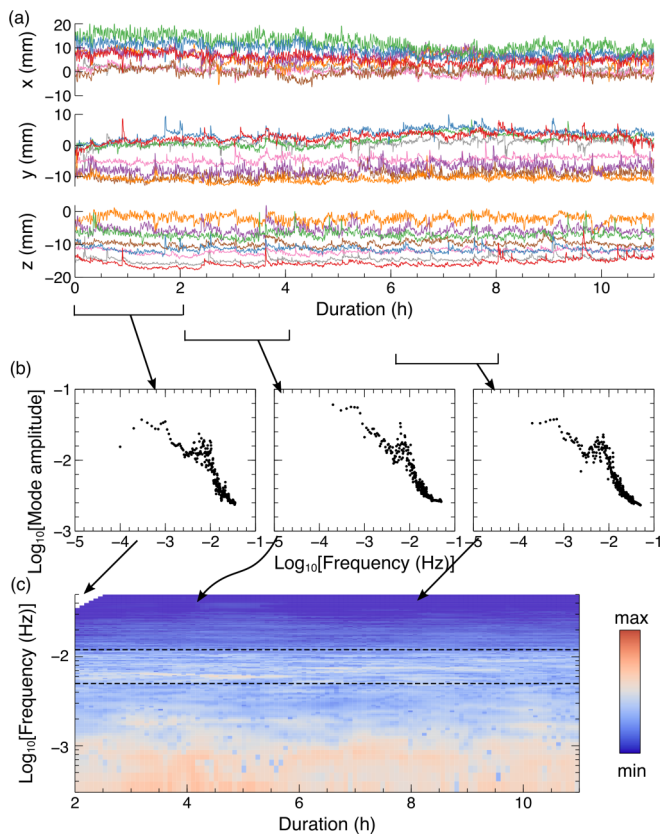


FIG. 3. Sliding-window DMD. (a) The raw motion signals of eight tentacles in terms of the x , y , and z coordinates are shown from top to bottom in different colors. (b) The DMD spectra of the corresponding segments of motion signals are shown from left to right. (c) The map formed by sliding-window DMD with the width = 120 min and translation = 5 min is shown. The arrows, from top to bottom, indicate the raw motion signals used to calculate the spectrum and indicate how the spectrum is oriented, respectively. The logarithm-scaled mode amplitude is encoded by the color.

window is chosen to be 720 (120 min), as shown by the brackets in Fig. 3(a). The raw data of tentacle position in the three-dimensional Cartesian coordinate system (x , y , z) is also shown in Fig. 3(a). Figure 3(b) displays three examples of a DMD spectrum of the windowed data. We notice that these spectra still preserve features of linear relation and peak area in the logarithm-scaled graph, implying that the $1/f^\alpha$ relation and modes with increased power near 0.008 Hz hold for these periods of tentacle motion. To see whether these features always exist in tentacle motions, we slide the window with a certain translation (5 min) and align these calculated DMD spectra to form a map similar to the spectrogram, where we can obtain the information in both time and frequency with adequate resolution, as shown in Fig. 3(c). The logarithm-scaled mode amplitude is encoded by the color. The visible trend is characterized by the mode amplitude being highest near zero frequency and decreasing as the frequency increases. Moreover, we observe the presence of spatial DMD modes with increased power in tentacle motion despite variation in a certain frequency range enclosed by black dashed lines (0.005–0.012 Hz). The maps formed by sliding-window DMD

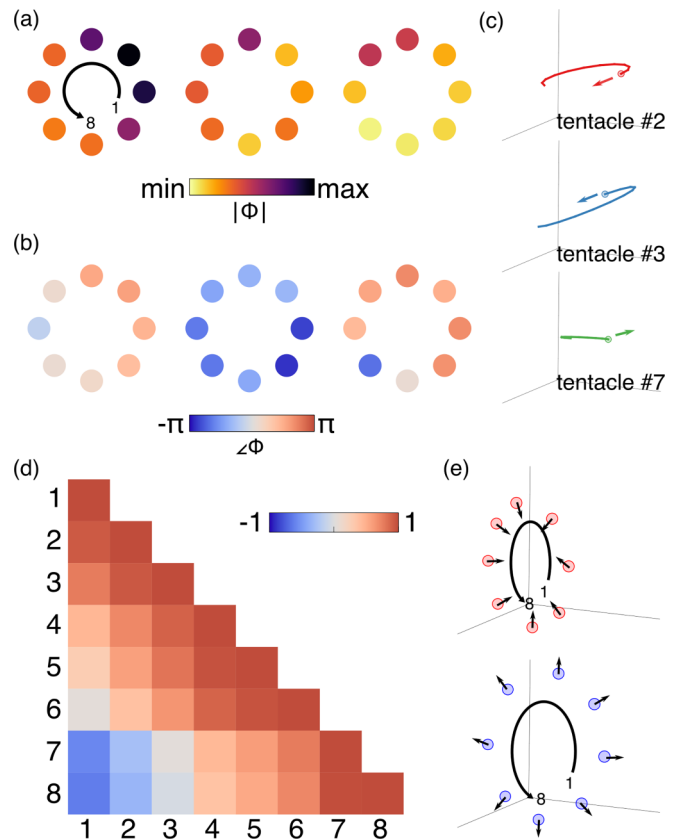


FIG. 4. The DMD modes of eight tentacles. (a) The magnitudes of DMD modes representing displacements along the x , y , and z directions are shown from left to right. The sequence of the tentacles is marked counterclockwise in the first panel. (b) The phases of DMD modes representing displacements along the x , y , and z directions are shown from left to right. (c) The reconstruction using the DMD mode shown in (a) and (b) illustrates the elliptical motions of tentacles with different angular velocities. The elliptical motions of tentacles #2, #3, and #7 with arrows indicating the moving directions are shown from left to right. (d) The correlation coefficients are calculated by the distances between each tentacle tip and central position of the tentacle crown. (e) The snapshots of pulsation motion when tentacles approach each other and when they are away from each other are shown from top to bottom, respectively. The sequence of the tentacles is marked counterclockwise.

in replicate experiments and under different light conditions show similarities and differences, as displayed in Fig. S2 in the Supplemental Material [24].

IV. CHARACTERIZATION OF DYNAMIC COHERENT PATTERNS

Since the tentacle motion always has DMD modes with increased power, it is natural to extract the spatial mode and examine the motion pattern. The mode with the largest amplitude between 0.005 and 0.012 Hz is chosen as the exemplar mode. Figures 4(a) and 4(b) exhibit the magnitude and phase of spatial DMD modes of eight tentacles marked counterclockwise by the sequence number, respectively. Specifically, the absolute values of displacements along the x , y , and z directions of the eight tentacles are shown from left to right

in Fig. 4(a). The waving motions along the x direction are distinct between tentacles but tentacles #1, #2, #3 and #4 have relatively large displacements compared with the others. This phenomenon is also reflected by the trajectories of eight tentacles in Fig. 1, where tentacles #1, #2, #3, and #4 have larger waving motions along the x direction than the other tentacles. The corresponding phases of displacement along the x direction are exhibited in the first panel of Fig. 4(b), where the phases of tentacles #1, #2, #3, and #4 are significantly greater than zero while others are close to or smaller than zero, implying that tentacles #1, #2, #3, and #4 approach and leave the others along the x direction rhythmically.

Likewise, the absolute values and phases of displacements along the y and z directions in the second and third panels of Figs. 4(a) and 4(b) can be interpreted. Displacements along the y and z directions are generally smaller than those along the x direction, indicating that the waving motion along the x direction is dominant. Displacements vary between tentacles and the largest displacements along the y and z directions are on tentacles #4 and #5, respectively. In contrast with tentacle displacement along the x direction, we notice that displacements along the y axis are in phase due to the consistent negative phases [the second panel in Fig. 4(b)], suggesting consistent tentacle motions towards the center of the tentacle crown. The displacements along the z axis, which represents the vertical waving motion, have the phase difference [the third panel in Fig. 4(b)]. The phases of tentacles #7 and #8 are close to or smaller than zero while the others are significantly greater than zero, suggesting that tentacles #1–#6 approach and leave the others along the z direction rhythmically.

Overall, this DMD mode is dominated by the displacement along the x direction and the displacement of tentacles #1–#5. Therefore, combined with the phase differences of the tentacles, we conclude that this spatial DMD mode represents the pulsation behavior of our pulsating soft coral. However, compared with the pulsation behaviors of the commonly studied Xeniid corals, *Xenia* and *Heteroxenia fuscescens*, where each tentacle moves close to the center almost synchronously with certain displacement resulting in the nearly symmetric pulsation process [21,22], *Anthelia glauca* pulsates by moving its tentacles with different displacements and different phases leading to an asymmetric pulsation process. Specifically, the tentacles #1–#5 have larger displacements while others have smaller displacement. Taking advantage of the phase difference along the x and z directions, tentacles approach and leave each other rhythmically. This pulsation behavior could have implications related to feeding, survival, and fitness of the colony, as it is known that the functions of pulsating soft coral tentacles may enhance photosynthesis and prey capture [14,21]. However, the specific biological functions of tentacle pulsation in different soft corals still need further exploration.

To further examine this specific DMD mode, next, we reconstructed the spatiotemporal motions of coral tentacles by only using the mode characterized above Φ , mathematically expressed as follows:

$$\hat{X} = \Phi \Lambda^{t-1} Z, \quad (8)$$

where the diagonal entries of Λ contain DMD eigenvalues and $Z = \Phi \backslash x_1$ (backslash to solve the linear system with MATLAB notation). x_1 is the initial position of the tentacles. Figure 4(c)

shows the 2-min trajectories of tentacles #2, #3, and #7 with the arrows indicating the direction of movement. The reconstruction of trajectories of eight tentacles with 200 time slots (around 33 min) is shown in the Supplemental Material (see Fig. S3) [24]. In general, the trajectories are ellipses that have polarizations along certain directions and the directions of the angular velocity of each tentacle are different. Since the eight tentacles are on the same tubular polyp, it is necessary to explore the pulsation relations among them.

We chose the distance between each tentacle tip and the central position of the tentacle crown from the reconstructed data to study the pulsation relation. When the tentacles approach each other, the distances will become smaller and vice versa. To show the pulsation relation, we calculate the correlation coefficient between the distance from tentacle m to the center and the distance from tentacle n to the center as follows:

$$r_{mn} = \frac{\sum (d_t^m - \bar{d}^m)(d_t^n - \bar{d}^n)}{\sqrt{\sum (d_t^m - \bar{d}^m)^2 \sum (d_t^n - \bar{d}^n)^2}}, \quad (9)$$

where t and the upper bar denote the time and the average of the temporal data. The positive correlation coefficient suggests that tentacles move towards or away from the center in synchrony, while the negative one indicates the opposite scenario, dyssynchronous movement. As shown in Fig. 4(d), most correlation coefficients are positive, indicating the collective pulsation motion. Tentacles #1 and #2 have negative correlation coefficients with tentacles #7 and #8. However, according to the Supplemental Material (see Fig. S3) [24], the displacements of tentacles #7 and #8 are quite small and thus have a small effect on the collective pulsation. The correlation analysis further confirms that this spatial DMD mode represents the pulsation behaviors by each tentacle collectively moving to or leaving from the center.

Figure 4(e) shows two snapshots when eight tentacles approach each other (the first panel) and when eight tentacles are away from each other (the second panel). By comparing two snapshots, tentacles #1–#4 have significant motion that coincides with our analysis above. In addition, these motions are dominant along the x direction, where the obvious closing and opening of the tentacle crown can be observed. As shown in the schematic in Supplemental Material Movie 2 ($\times 300$ speed) [24], the periodic closing and opening of the tentacles results from the reciprocating elliptical motion of each tentacle. The sizes of elliptical trajectories become smaller gradually because of this decaying mode (the absolute value of the eigenvalue of this mode is smaller than 1). In reality, the pulsation behavior is accompanied with our soft coral, resulting in the stable oscillating mode where the absolute value of the eigenvalue should be 1. This may result from the error of this numerical reconstruction.

A series of snapshots over time illustrating the closing and opening process of the tentacle crown are shown in the Supplemental Material (Fig. S4) [24]. The tentacle motion described here could be leveraged to further study fluid dynamics in soft coral colonies in relation to enhance photosynthesis of the symbiotic algae and prevent refiltration of surrounding water by neighboring polyps [20–22]. Note that the extracted pulsation motion of our soft coral is not as

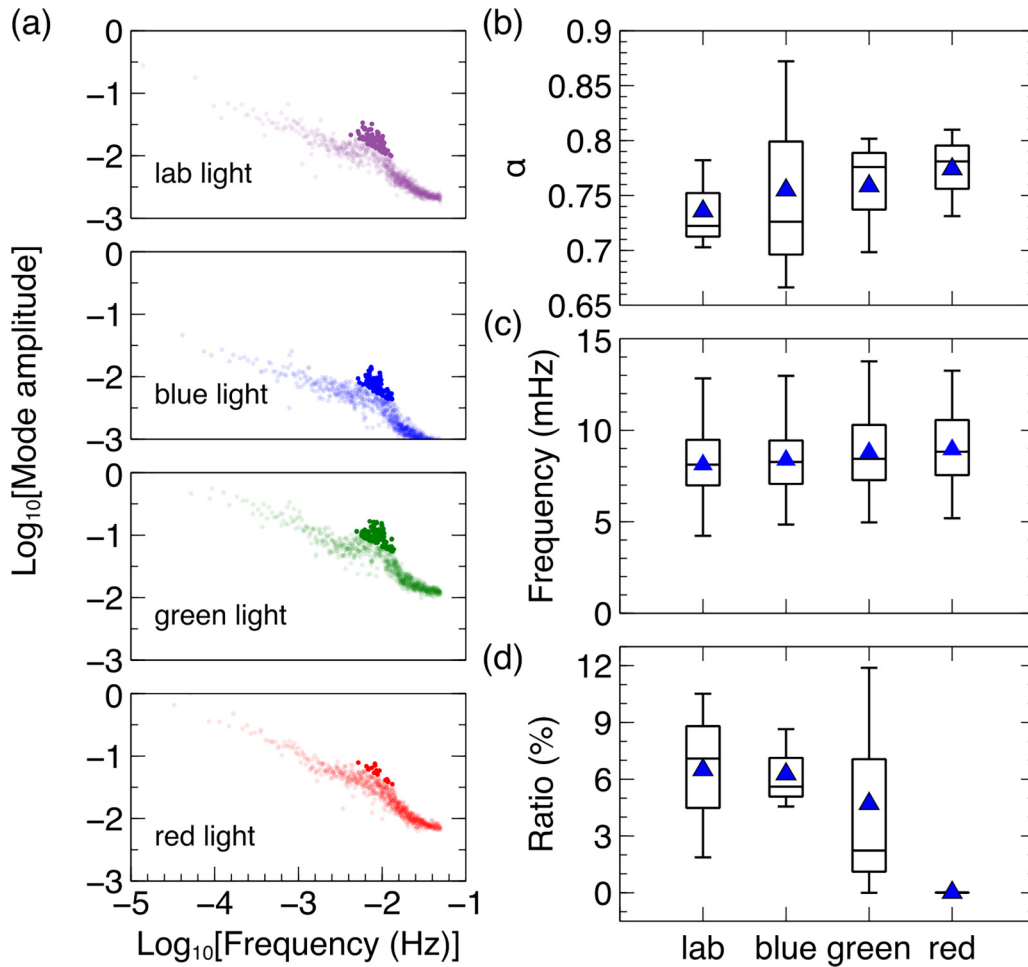


FIG. 5. The effect of light conditions on the DMD modes. (a) The DMD spectra under different light wavelengths are shown from top to bottom. The light in different colors in each graph represent modes with magnitudes within $1/f^\alpha$ fit, while the dark colors represent those exceeding the criteria of $1/f^\alpha$ fit. (b) The power α under different light wavelengths. (c) The frequencies of the spatial DMD modes with pulsation under different light wavelengths. (d) The ratio of the number of spatial DMD modes with pulsation under different light wavelengths. The blue triangles represent the mean of the data in (b), (c), and (d).

obvious and powerful as that of the widely studied pulsating *Xenia* coral, which coincides with the characteristics of *Anthelia glauca*. In addition, from this study, DMD demonstrates the capability of extracting the weak pulsation modes from $1/f$ noise.

V. EFFECT OF LIGHT CONDITIONS

So far, we have focused the analysis on the pulsating soft coral under the light conditions in our laboratory. However, environmental variables, such as the wavelength of light, are known to have impacts on coral behaviors [11,12,31,32]. Therefore, it is interesting to investigate whether different wavelengths of light can affect pulsation behaviors. Figure 5(a) shows the DMD spectra obtained under the laboratory light: blue, green, and red from top to bottom, respectively. The linear trend in the logarithm-scaled graph and the area with increased power still exist when the light condition changes to light in other colors. Note that regression and mode detection are the same here as above; however, some differences can be observed such as the slope, frequency range, and the number of modes with pulsation. To investigate the

effect of variation in the color of light, each light treatment experiment was replicated three times while keeping other conditions the same.

Figure 5(b) shows the power α as a function of light wavelength. α slightly increases with increasing wavelength on average, suggesting that the low-frequency modes have more power when the light condition shifts to red light. But no significant difference is found according to the p value. The frequency ranges of DMD pulsation modes under different light conditions are shown in Fig. 5(c), where no significant differences are visible according to the p value. Hence, the wavelength of light does not appear to have a major impact on the frequency range of the pulsation behaviors. In addition, the number of modes with pulsation detected using our criteria is normalized by the total number of modes, which is visualized in Fig. 5(d) as the ratio. As the wavelength increases from blue to red, the ratio declines on average. Specifically, when the light condition shifts to red, the number of DMD pulsation modes drops significantly to almost zero, indicating the submergence of these DMD pulsation modes into the $1/f$ noise. Under the red light, the number of DMD pulsation modes is significantly different from that in the other

light conditions tested ($p < 0.05$). Moreover, this trend can be observed from the map formed by the sliding-window DMD shown in the Supplemental Material (Fig. S2) [24], where the corresponding modes nearly disappear as the light shifts to red. This indicates dormant pulsation behavior under red light conditions. Here is one possible interpretation of this result. *Anthelia glauca* is found to live deeper than many other soft corals, so the red light is difficult to reach and photosynthesis is limited [33]. The pulsation motion is able to capture food particles in the water or obtain dissolved matter from the surrounding water as a source of energy [13–15]. When there exists sufficient red light, there is probably little need for pulsation motion to catch prey, which will submerge into the $1/f$ -type motion, resulting in the increasing low-frequency modes (increasing α).

VI. CONCLUSION AND DISCUSSION

In our study, stereovision is used to capture the motion of the eight tentacles forming the crown of one polyp of the pulsating soft coral, *Anthelia glauca*. The stochastic motion is revealed taking advantage of the use of synchronized dual cameras. Dynamic mode decomposition, a data-driven method, is used to analyze the growth/decay and oscillation involved in this process. Therein, the $1/f$ -type motion is identified in the tentacle motion, which is common in biological systems. Furthermore, the DMD spatial modes with increased power constantly appearing in tentacle motion are captured in the DMD spectrum. We also visualize these spatial modes in terms of magnitude and phase, along with the correlation analysis among elliptical motions of tentacles, to confirm that these spatial modes represent the pulsation behaviors of soft corals of the Xenidiidae family. Moreover, we find clear evidence that the wavelength of light has impacts on the $1/f$ -type motion and the emergence of pulsation behaviors. Specifically, the red light plays an important role in ma-

nipulating the pulsation behaviors, which shares the similar phenomenon with the polyps of *Pocillopora acuta* (stony coral) under the impact of red light [12].

Anthelia glauca pulses far less than *Xenia* corals do, in addition to the emergence of the pulsation behaviors in the $1/f$ -type motion in our study, which results in the difficulty in observing pulsation directly from the field and aquarium. However, our data-driven method successfully extracts the pulsation mode, demonstrating the ability of DMD. Note that our experiment is conducted without the seawater flow, which opens up the following application of DMD on the more practical scenario with the seawater flow in the field or aquarium. Additionally, every individual tentacle has a special mode and behaves differently, which inspires the further exploration of biological neuron structures in pulsating soft corals. In the same phylum of cnidarians owning the diffuse nervous system that coordinates behaviors, sea anemones can be a good example to guide a similar study in tentacles motion [34].

Our proposed data-driven method, DMD, can be a powerful tool for the analysis, understanding, and extraction of the attractive behaviors of pulsating soft corals. Our study also broadens the applications of DMD, which is applied to the field of coral behaviors. In the future study, the DMD method could be expanded beyond the motion analysis by correlating spatiotemporal behaviors of animals with the corresponding spatiotemporal measurement.

ACKNOWLEDGMENTS

We acknowledge financial support by the U.S. National Science Foundation (HDR: DIRSE-IL, Grants No. 1939249, No. 1940169, No. 1939699, and No. 1939263). J.Y. also acknowledges support from the SNU-IAMD, SNU-IOER, and the Brain Pool Plus program funded by the Ministry of Science and ICT through the National Research Foundation of Korea (2022H1D3A2A03096579).

-
- [1] J. N. Kutz, Deep learning in fluid dynamics, *J. Fluid Mech.* **814**, 1 (2017).
 - [2] D. Kochkov, J. A. Smith, A. Alieva, Q. Wang, M. P. Brenner, and S. Hoyer, Machine learning–accelerated computational fluid dynamics, *Proc. Natl. Acad. Sci. USA* **118**, e2101784118 (2021).
 - [3] D. Rolnick, P. L. Donti, L. H. Kaack, K. Kochanski, A. Lacoste, K. Sankaran, A. S. Ross, N. Milojevic-Dupont, N. Jaques, A. Waldman-Brown *et al.*, Tackling climate change with machine learning, *ACM Comput. Surv.* **55**, 96 (2023).
 - [4] C. W. Rowley, I. Mezi, S. Bagheri, P. Schlatter, and D. S. Henningson, Spectral analysis of nonlinear flows, *J. Fluid Mech.* **641**, 115 (2009).
 - [5] P. J. Schmid, Dynamic mode decomposition of numerical and experimental data, *J. Fluid Mech.* **656**, 5 (2010).
 - [6] E. Berger, M. Sastuba, D. Vogt, B. Jung, and H. Ben Amor, Estimation of perturbations in robotic behavior using dynamic mode decomposition, *Adv. Robot.* **29**, 331 (2015).
 - [7] B. W. Brunton, L. A. Johnson, J. G. Ojemann, and J. N. Kutz, Extracting spatial-temporal coherent patterns in large-scale neural recordings using dynamic mode decomposition, *J. Neurosci. Methods* **258**, 1 (2016).
 - [8] Y. Shiraishi, Y. Kawahara, O. Yamashita, R. Fukuma, S. Yamamoto, Y. Saitoh, H. Kishima, and T. Yanagisawa, Neural decoding of electrocorticographic signals using dynamic mode decomposition, *J. Neural Eng.* **17**, 036009 (2020).
 - [9] J. L. Proctor and P. A. Eckhoff, Discovering dynamic patterns from infectious disease data using dynamic mode decomposition, *Int. Health* **7**, 139 (2015).
 - [10] D. R. Bellwood, T. P. Hughes, C. Folke, and M. Nyström, Confronting the coral reef crisis, *Nature (London)* **429**, 827 (2004).
 - [11] S. Li, L. M. Roger, L. Kumar, N. A. Lewinski, J. Klein-Seetharaman, A. Gagnon, H. M. Putnam, and J. Yang, Digital image processing to detect subtle motion in stony coral, *Sci. Rep.* **11**, 7722 (2021).
 - [12] S. Li, L. M. Roger, J. Klein-Seetharaman, N. A. Lewinski, and J. Yang, Spatiotemporal Dynamics of Coral Polyps on a Fluidic Platform, *Phys. Rev. Appl.* **18**, 024078 (2022).
 - [13] D. Schlichter, Epidermal nutrition of the alcyonarian *Heteroxenia fuscescens* (Ehrb.): Absorption of dissolved organic material and lost endogenous photosynthates, *Oecologia* **53**, 40 (1982).
 - [14] J. B. Lewis, Feeding behaviour and feeding ecology of the Octocorallia (Coelenterata: Anthozoa), *J. Zool.* **196**, 371 (1982).

- [15] K. E. Fabricius and D. W. Klumpp, Widespread mixotrophy in reef-inhabiting soft corals: The influence of depth, and colony expansion and contraction on photosynthesis, *Mar. Ecol. Prog. Ser.* **125**, 195 (1995).
- [16] E. D. Lapid, J. Wielgus, and N. E. Chadwick-Furman, Sweeper tentacles of the brain coral *Platygyra daedalea*: Induced development and effects on competitors, *Mar. Ecol. Prog. Ser.* **282**, 161 (2004).
- [17] D. Malul, R. Holzman, and U. Shavit, Coral tentacle elasticity promotes an out-of-phase motion that improves mass transfer, *Proc. R. Soc. B* **287**, 20200180 (2020).
- [18] C. O. Pacherres, S. Ahmerkamp, G. M. Schmidt-Grieb, M. Holtappels, and C. Richter, Ciliary vortex flows and oxygen dynamics in the coral boundary layer, *Sci. Rep.* **10**, 7541 (2020).
- [19] O. H. Shapiro, V. I. Fernandez, M. Garren, J. S. Guasto, F. P. Debailon-Vesque, E. Kramarsky-Winter, A. Vardi, and R. Stocker, Vortical ciliary flows actively enhance mass transport in reef corals, *Proc. Natl. Acad. Sci. USA* **111**, 13391 (2014).
- [20] C. Wild and M. S. Naumann, Effect of active water movement on energy and nutrient acquisition in coral reef-associated benthic organisms, *Proc. Natl. Acad. Sci. USA* **110**, 8767 (2013).
- [21] M. Kremien, U. Shavit, T. Mass, and A. Genin, Benefit of pulsation in soft corals, *Proc. Natl. Acad. Sci. USA* **110**, 8978 (2013).
- [22] J. E. Samson, L. A. Miller, D. Ray, R. Holzman, U. Shavit, and S. Khatri, A novel mechanism of mixing by pulsing corals, *J. Exp. Biol.* **222**, jeb192518 (2019).
- [23] T. L. Hedrick, Software techniques for two- and three-dimensional kinematic measurements of biological and biomimetic systems, *Bioinspir. Biomim.* **3**, 034001 (2008).
- [24] See Supplemental Material at <http://link.aps.org/supplemental/10.1103/PhysRevResearch.5.013175> for the DMD reconstruction error, sliding-window DMD, and the reconstruction of pulsation motion.
- [25] M. Kamb, E. Kaiser, S. L. Brunton, and J. Nathan Kutz, Time-delay observables for Koopman: Theory and applications, *SIAM J. Appl. Dyn. Syst.* **19**, 886 (2020).
- [26] V. M. N. C. S. Vieira, J. Creed, R. A. Scrosati, A. Santos, G. Dutschke, F. Leitão, A. H. Engelen, O. R. Huanel, M. L. Guillemin, M. Mateus, and R. Neves, On the choice of linear regression algorithms for biological and ecological applications, *Annu. Res. Rev. Biol.* **10**, 1 (2016).
- [27] C. Bédard, H. Kröger, and A. Destexhe, Does the $1/f$ Frequency Scaling of Brain Signals Reflect Self-Organized Critical States? *Phys. Rev. Lett.* **97**, 118102 (2006).
- [28] K. J. Miller, L. B. Sorensen, J. G. Ojemann, and M. Den Nijs, Power-law scaling in the brain surface electric potential, *PLoS Comput. Biol.* **5**, e1000609 (2009).
- [29] L. S. Tsimring, Noise in biology, *Rep. Prog. Phys.* **77**, 026601 (2014).
- [30] P. Szendro, G. Vincze, and A. Szasz, Pink-noise behaviour of biosystems, *Eur. Biophys. J.* **30**, 227 (2001).
- [31] P. P. Laissue, L. Roberson, Y. Gu, C. Qian, and D. J. Smith, Long-term imaging of the photosensitive, reef-building coral *Acropora muricata* using light-sheet illumination, *Sci. Rep.* **10**, 10369 (2020).
- [32] T. Wijgerde, A. Van Melis, C. I. F. Silva, M. C. Leal, L. Vogels, C. Mutter, and R. Osinga, Red light represses the photophysiology of the scleractinian coral *Stylophora pistillata*, *PLoS ONE* **9**, e92781 (2014).
- [33] Y. Benayahu and Y. Loya, Competition for space among coral-reef sessile organisms at Eilat, Red Sea, *Bull. Mar. Sci.* **31**, 514 (1981).
- [34] J. A. Westfall, C. F. Elliott, and R. W. Carlin, Ultrastructural evidence for two-cell and three-cell neural pathways in the tentacle epidermis of the sea anemone *Aiptasia pallida*, *J. Morphol.* **251**, 83 (2002).